Dissipationless Anomalous Hall Current in the Ferromagnetic Spinel $CuCr_2Se_{4-x}Br_x$.[*]

Wei-Li Lee[1], Satoshi Watauchi[2†], V. L. Miller[2], R. J. Cava[2,3], and N. P. Ong[1,3‡]

[1]*Department of Physics,* [2]*Department of Chemistry,*
[3]*Princeton Materials Institute, Princeton University, New Jersey 08544, U.S.A.*
(Dated: February 2, 2008)

In a ferromagnet, an applied electric field $\mathbf{E}$ invariably produces an anomalous Hall current $\mathbf{J}_H$ that flows perpendicular to the plane defined by $\mathbf{E}$ and $\mathbf{M}$ (the magnetization). For decades, the question whether $\mathbf{J}_H$ is dissipationless (independent of the scattering rate), has been keenly debated without experimental resolution. In the ferromagnetic spinel $CuCr_2Se_{4-x}Br_x$, the resistivity ρ (at low temperature) may be increased 1000 fold by varying x(Br), without degrading the $\mathbf{M}$. We show that $\mathbf{J}_H/E$ (normalized per carrier, at 5 K) remains unchanged throughout. In addition to resolving the controversy experimentally, our finding has strong bearing on the generation and study of spin-Hall currents in bulk samples.

A major unsettled question in the study of electron transport in a ferromagnet is whether the anomalous Hall current is dissipationless. In non-magnetic metals, the familiar Hall current arises when electrons moving in crossed electric ($\mathbf{E}$) and magnetic ($\mathbf{H}$) fields are deflected by the Lorentz force. However, in a ferromagnet subject to $\mathbf{E}$ alone, a large, spontaneous (anomalous) Hall current $\mathbf{J}_H$ appears transverse to $\mathbf{E}$ (in practice, a weak $\mathbf{H}$ serves to align the magnetic domains) *(1,2)*. Questions regarding the origin of $\mathbf{J}_H$, and whether it is dissipationless, have been keenly debated for decades. They have emerged anew because of fresh theoretical insights and strong interest in spin currents for spin-based electronics. Here we report measurements in the ferromagnet $CuCr_2Se_{4-x}Br_x$ which establish that, despite a 100-fold increase in the scattering rate from impurities, $\mathbf{J}_H$ (per carrier) remains constant, implying that it is indeed dissipationless.

In 1954, Karplus and Luttinger (KL)*(3,4)* proposed a purely quantum-mechanical origin for $\mathbf{J}_H$. An electron in the conduction band of a crystal lattice spends part of its time in nearby bands because of admixing caused by the (intracell) position operator $\mathbf{X}$. In the process, it acquires a spin-dependent 'anomalous velocity' *(5)*. KL predicted that the Hall current is dissipationless: $\mathbf{J}_H$ remains constant even as the longitudinal current ($\mathbf{J}||\mathbf{E}$) is degraded by scattering from added impurities. A conventional mechanism was later proposed *(6)* whereby the anomalous Hall effect (AHE) is caused instead by asymmetric scattering of electrons by impurities (skew scattering). Several authors *(7,8,9)* investigated the theoretical ramifications of these competing models. The role of impurities in the anomalous-velocity theory was clarified by Berger's side-jump model *(7)*. A careful accounting of various contributions (including side-jump) to the

AHE in a semiconductor has been given by Nozières and Lewiner (NL) who derive $\mathbf{X} = \lambda \mathbf{k} \times \mathbf{S}$, with λ the enhanced spin-orbit parameter, $\mathbf{k}$ the carrier wavevector and $\mathbf{S}$ its spin *(9)*. In the dc limit, NL obtain the AHE current

$$\mathbf{J}_H = 2ne^2\lambda\mathbf{E} \times \mathbf{S}, \qquad (1)$$

where n is the carrier density and e the charge. As noted, $\mathbf{J}_H$ is linear in $\mathbf{S}$ but independent of the electron lifetime τ.

In modern terms, the anomalous velocity term of KL is related to the Berry phase *(10)*, and has been applied *(11)* to explain the AHE in Mn-doped GaAs *(12)*. The close connection of the AHE to the Berry phase has also been explored in novel ferromagnets in which frustration leads to spin chirality *(13,14,15)*. In the field of spintronics, several schemes have been proposed to produce a fully polarized spin current in thin-film structures *(16)*, and in bulk p-doped GaAs *(17)*. The AHE is intimately related to these schemes, and our experimental results have bearing on the spin-current problem.

In an AHE experiment *(1)*, the observed Hall resistivity is comprised of two terms,

$$\rho_{xy} = R_0 B + \rho'_{xy}, \qquad (2)$$

with B the induction field, R_0 the ordinary Hall coefficient, and ρ'_{xy} the anomalous Hall resistivity. A direct test of the dissipationless nature of $\mathbf{J}_H$ is to check whether the anomalous Hall conductivity σ'_H (defined as ρ'_{xy}/ρ^2) changes as impurities are added to increase $1/\tau$ (and ρ) *(3,7)*. A dissipationless AHE current implies that $\rho'_{xy} \sim \rho^\alpha$, with $\alpha = 2$. By contrast, in the skew scattering model, $\alpha = 1$.

Tests based on measurements at high temperatures (77-300 K) yield exponents in the range $\alpha_{exp} = 1.4$-2.0 *(18,19)*. However, it has been argued *(20)* that, at high T, both models in fact predict $\alpha = 2$, a view supported by detailed calculations *(21)*. To be meaningful, the test must be performed in the impurity-scattering regime over a wide range of ρ. Unfortunately, in most ferromagnets, ρ'_{xy} becomes too small to measure accurately at low T. Results on α in the impurity-scattering regime are very limited.

The copper-chromium selenide spinel $CuCr_2Se_4$, a metallic ferromagnet with a Curie temperature $T_C \sim$ 430 K, is particularly well-suited for testing the AHE. Substituting Se with Br in $CuCr_2Se_{4-x}Br_x$ decreases the hole density n_h (22). However, because the coupling between local moments on Cr is primarily from 90° superexchange along the Cr-Se-Cr bonds (23), this does not destroy the magnetization. We have grown crystals of $CuCr_2Se_{4-x}Br_x$ by chemical vapor transport [details given in Supporting Online Materials (SOM) (24)]. Increasing x from 0 to 1 in our crystals decreases n_h by a factor of ~30 (Fig. 1A), while T_C decreases from 430 K to 230 K. The saturated magnetization M_s at 5 K corresponds to a Cr moment that actually increases from ~2.6 to 3 μ_B (Bohr magneton) (Fig. 1B).

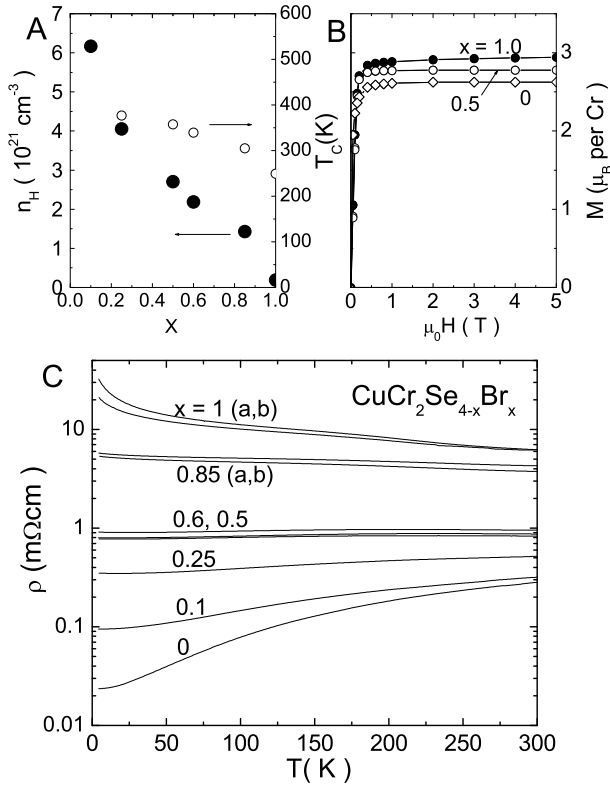~270, as x increases from 0 to 0.85, and is predominantly due to a 70-fold decrease in τ. The hole density n_h decreases by only a factor of 4. In the localization regime ($x = 1.0$), strong disorder causes ρ to rise gradually with decreasing T. We emphasize, however, that these samples are not semiconductors (ρ is not thermally activated, and $n_h = 1.9 \times 10^{20}$ cm^{-3} is degenerate).

The field dependence of the total Hall resistivity (Eq. 2) is shown for $x = 0.25$ (Fig. 2A) and 1.0 (B). See SOM (24) for measurement details. The steep increase in $|\rho_{xy}|$ in weak H reflects the rotation of domains into alignment with $\mathbf{H}$. Above the saturation field H_s, when ρ'_{xy} is constant, the small ordinary Hall term $R_0 B$ is visible as a linear background (24). As in standard practice, we used R_0 measured above T_C to find the n_h plotted in Fig. 1A.
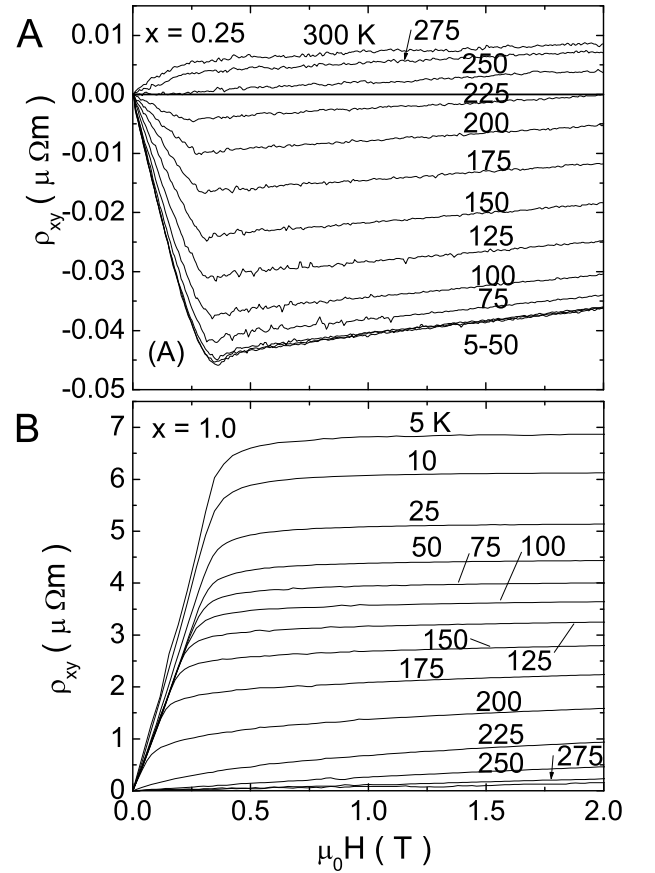

FIG. 1: (A) The hole density n_h (solid circles) in $CuCr_2Se_{4-x}Br_x$ vs. x determined from R_0 at 400 K (one hole per formula unit corresponds to $n_h = 7.2 \times 10^{21}$cm^{-3}). The Curie temperature T_C is shown as open circles. (B) Curves of the magnetization M vs. H at 5 K in 3 samples (x values indicated). The saturation value $M_s = 3.52, 3.72, 3.95$ (10^5A/m) for $x = 0, 0.5, 1.0$, respectively. (C) The resistivity ρ vs. T in 10 samples with Br content x indicated (a, b indicate different samples with the same x). Values of n_h in all samples fall in the metallic regime (for $x = 1$, $n_h = 1.9 \times 10^{20}$ cm^{-3}).

FIG. 2: Curves of the observed Hall resistivity $\rho_{xy} = R_0 B + R_s \mu_0 M$ vs. H (at temperatures indicated) in $CuCr_2Se_{4-x}Br_x$ with $x = 0.25$ (Panel A) and $x = 1.0$ (B). In (A), the anomalous Hall coefficient R_s changes sign below 250 K, becomes negative, and saturates to a constant value below 50 K. However, in (B), R_s is always positive and rises to large values at low T (note difference in scale).

As shown in Fig. 1C, all samples except the ones with $x = 1.0$ lie outside the localization regime. In the 'metallic' regime, the low-T resistivity increases by a factor of

By convention, the T dependence of the AHE signal is represented by the anomalous Hall coefficient $R_s(T)$ defined by $\rho'_{xy} = R_s \mu_0 M$ (μ_0 is the vacuum permeability).
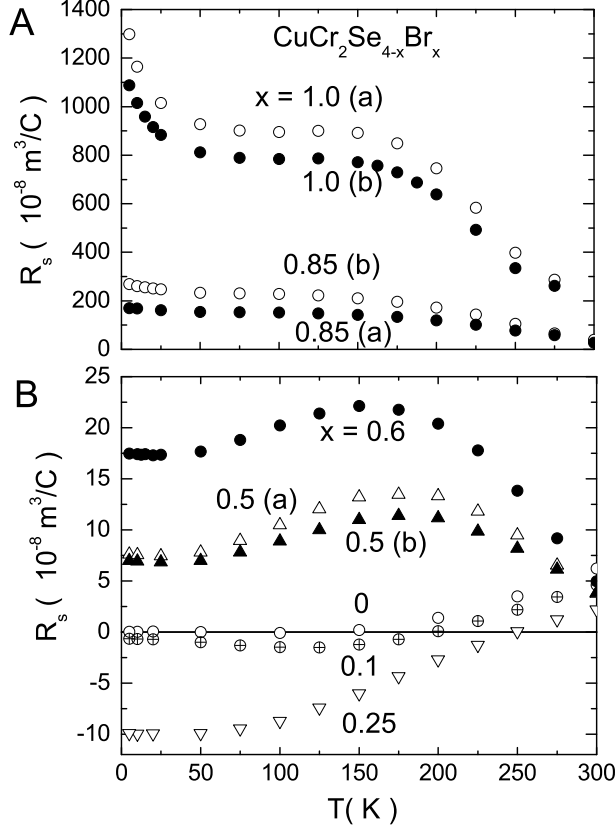
FIG. 3: (A) Values of R_s extracted from the curves of ρ_{xy} and M vs H measured at each T in $CuCr_2Se_{4-x}Br_x$ with values of x indicated (a and b refer to different crystals with the same x). The corresponding curves for $x = 0$, 0.1, 0.25 and 0.5 (2 crystals a and b) are displayed in Panel (B). The values of R_s at 5 K are negative at small x (< 0.4), but as x increases, R_s rapidly rises to large positive values.

By scaling the ρ'_{xy}-H curve against the M-H curve measured at each T, we have determined (24) R_s vs. T in each of the samples studied (Fig. 3). The introduction of Br causes the R_s vs. T profiles to change dramatically. In the undoped sample ($x = 0$), R_s is positive and monotonically decreasing below 360 K, as typical in high-purity ferromagnets (Fig. 3B). Weak doping ($x = 0.1$) produces a negative shift in R_s and a finite negative value at low T. Increasing the doping to $x = 0.25$ leads to an R_s profile that is large, negative and nearly T independent below 50 K (Fig. 2A). At mid-range doping and higher ($x \geq 0.5$), the magnitude of R_s increases steeply, but now in the positive direction. At maximum doping ($x = 1$), the value of R_s at 5 K is very large, corresponding to $\rho'_{xy} \sim 700$ $\mu\Omega$cm (Fig. 2A).

Our focus is on the low-T values of ρ'_{xy} where impurity scattering dominates. At 5 K, ρ'_{xy} is too small to be resolved in the sample with $x = 0$. As x increases to 1, the absolute magnitude $|\rho'_{xy}|$ at 5 K increases by over 3

orders of magnitude (from hereon ρ'_{xy} refers to the saturated value measured at 2 Teslas or higher). Significantly, ρ'_{xy} is negative at low doping ($0 < x < 0.4$), but becomes positive for $x > 0.5$. Initially, the sign-change seemed to suggest to us that there might exist 2 distinct mechanisms for the AHE in this system. As more samples were studied, however, it became apparent that, regardless of the sign, the magnitude $|\rho'_{xy}|$ versus ρ falls on the same curve over several decades (Fig. 4), providing strong evidence that the same AHE mechanism occurs in both sign regimes. We focus first on the magnitude $|\rho'_{xy}|$ vs. ρ, and discuss the change in sign later.

It is worth emphasizing that σ'_H is proportional to the carrier density n_h (see Eq. 1). For our goal of determining whether the AHE current is dissipationless, it is clearly necessary to factor out n_h before comparing ρ'_{xy} against ρ. Hence we divide $|\rho'_{xy}|$ by n_h. We refer to σ'_H/n_h as the normalized AHE conductivity (24).
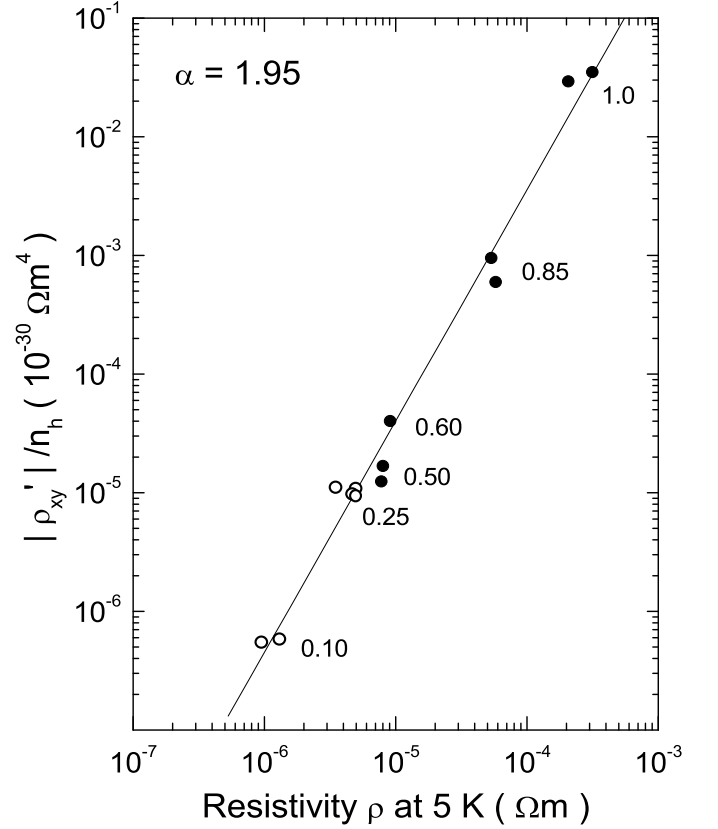

FIG. 4: The normalized quantity $|\rho'_{xy}|/n_h$ versus ρ (at 5 K) in a log-log plot (ρ'_{xy} is measured at 2 T and 5 K). The 12 samples (with doping x indicated) include ones with negative ρ'_{xy} (open circles) and positive ρ'_{xy} (solid). The undoped sample ($x = 0$) is not shown because ρ'_{xy} at 5 K is unresolved in our experiment (24). The least-squares fit gives $\rho'_{xy}/n_h = \mathcal{A}\rho^\alpha$ with $\mathcal{A} = 2.24 \times 10^{-25}$ (SI units) and $\alpha = 1.95 \pm 0.08$.

Figure 4 displays $|\rho'_{xy}|/n_h$ versus ρ in log-log scale

for all samples investigated (except $x = 0$). Over several decades, the data fit well to $|\rho'_{xy}|/n_h = \mathcal{A}\rho^\alpha$ with $\alpha = 1.95 \pm 0.08$ (as M_s is nearly insensitive to x, Fig. 4 also gives $R_s/n_h \sim \rho^2$). This immediately implies that the normalized AHE conductivity σ_H/n_h at 5 K is dissipationless. Increasing ρ by a factor of ~ 100 leaves the AHE current per carrier unchanged to our measurement accuracy [see SOM (24) for a discussion of our resolution]. As noted, the 2 samples with $x = 1$ are in the localization regime. The fact that their points also fall on the line implies that the dissipationless nature of the normalized AHE current extends beyond the Bloch-state regime (where most AHE theories apply) into the weak localization regime, where much less has been done. This supports recent theories (10,11,17) that the anomalous velocity origin is topological in nature, and equally valid in the Bloch and localization regimes.

The sign change at $x \sim 0.4$ is reminiscent of sign changes observed in ferromagnetic alloys (versus composition). The common feature is that doping drives the Fermi energy ϵ_F across the overlap between two narrow bands derived from distinct transition-metal elements. In the alloy $Ni_{1-x}Fe_x$, the band derived from Fe $3d$ states lies just above the $3d$ band of Ni. As ϵ_F crosses the overlap, ρ'_{xy} changes from negative to positive. Similar sign changes are observed in Au-Fe and Au-Ni alloys. It has been pointed out (2) that the spin-orbit parameter λ in Eq. 1 changes sign whenever ϵ_F moves between overlapping narrow bands. A similar effect is implied in NL's calculation (9). Band-structure calculations (25) on $CuCr_2Se_4$ reveal that ϵ_F lies in a hole-like band of mostly Cu $3d$ character strongly admixed with Cr $3d$ states lying just above. We infer that, as ϵ_F rises with increasing Br content, the conduction states acquire more Cr $3d$ character at the expense of Cu $3d$, triggering a sign-change in λ. The sign change (negative to positive with increasing x) is consistent with that observed in $Ni_{1-x}Fe_x$. A change-in-sign of the AHE conductivity at band crossings is also described in recent theories (10).

We now discuss the relevance of our findings to spin-current production. To produce fully polarized spin currents, it is ideal to use 'half metals' (ferromagnets in which all conduction electrons are, say, spin-up). However, only a few examples are known (26). Alternate schemes based on elemental ferromagnets have been proposed (16). As evident from Eq. 1, anomalous-velocity theories predict that $\mathbf{J}_H$ depends on the carrier spin $\mathbf{S}$. If a beam of electrons with spin populations $n_\uparrow$ and $n_\downarrow$ enters a region of fixed $\mathbf{M}$, the spin-up and spin-down electrons are deflected in opposite directions transverse to $\mathbf{E}$, just as in the classic Stern-Gerlach experiment. This results in a Hall charge current proportional to the difference between the spin populations, viz. $\mathbf{J}_H \sim (n_\uparrow - n_\downarrow)$. More importantly, this also produces a fully polarized spin Hall current $\mathbf{J}_s$ proportional to the sum $(n_\uparrow + n_\downarrow)$. Hence, in a ferromagnet that is not a half metal, the spin Hall current is fully polarized according to these theories. By contrast, in skew-scattering theories, $\mathbf{J}_H$ depends on

the direction of the local moment $\mathbf{m}_i$ on the impurity but not the spin of the incident electron (i.e. both J_H and $J_s \sim (n_\uparrow - n_\downarrow)$).

In confirming that the normalized AHE current is dissipationless over a multi-decade change in ρ, we verify a specific prediction of the anomalous-velocity theories and resolve a key controversy in ferromagnets. The implication is then that fully polarized spin-Hall currents are readily generated in ferromagnets (at low T) by simply applying $\mathbf{E}$. While this realization does not solve the conductivity-mismatch problem at interfaces (27), it may greatly expand the scope of experiments on the properties of spin currents.

Supporting Online Material
Materials and Methods
Mixtures of Cu, Cr, Se and $CuBr_2$ powder were heated at 550-600ºC for 20 h in evacuated sealed quartz tubes. The reactants ($\sim$3 g) were pulverized and sealed in quartz tubes (1.4×15 cm) with iodine ($\sim$0.3 g) as the transport gas for the crystal growth. The temperature gradient was fixed at 6.7ºC/cm (ends at $\sim$870 and $\sim$770 ºC) during the 2-week period of growth. The Br content was analyzed by EDX spectroscopy. For the Hall measurements, samples of typical size $1.5 \times 0.5 \times 0.1$ mm^3 were cut from as-grown crystals.

Measurements and analysis
On each crystal, microspots of indium solder were used to attach a pair of current I leads and 2 pairs of transverse voltage V leads in the standard Hall-bar geometry. The Hall voltage V_{xy} was measured (by ac phase-sensitive detection) in a field swept from -2 T to +2 T at the rate 5 mT/s. The value of I equals 1 mA for samples with $0 \leq x < 0.5$, and 0.1 mA for $0.5 \leq x \leq 1$. The Hall resistivity is calculated from the antisymmetric part of the Hall voltage, viz. $\rho_{xy} = [V_{xy}(H) - V_{xy}(-H)]/2I$ to remove the "IR" drop from Hall lead misalignment (typically, the "IR" background, which is symmetric in H, accounts for less than 5% of the recorded Hall voltage). In most samples, we checked for current uniformity by comparing the Hall signals from the 2 pairs of Hall voltage leads. The two signals agree to better than 5%. The largest source of error arises from measurements of the crystal thickness and the finite size of the microdot contacts (which affect the effective length and width). We estimate that these geometric errors contribute ± 7 % to the uncertainty in the absolute values of ρ_{xy} and ρ.
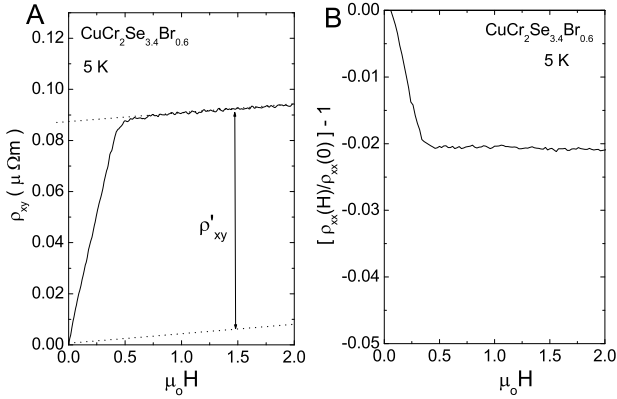

FIG. 5: (Panel A) Trace of ρ_{xy} vs. H in $CuCr_2Se_{4-x}Br_x$ ($x = 0.6$) obtained by antisymmetrizing the recorded Hall voltage. The linear background (broken line) is the term R_0B in Eq. 3. The AHE resistivity ρ'_{xy} is indicated by double arrow. Panel B shows the weak magnetoresistance of the same sample at 5 K. The fractional decrease $\rho(H)/\rho(0) - 1$ is $\sim$ 2%.

Figure 5 shows a 'raw' trace of the observed Hall resis-

tivity vs. H at $T = 5$ K in a crystal with $x = 0.6$. The trace is consistent with the equation

$$\rho_{xy} = R_0B + \rho'_{xy}, \qquad (\rho'_{xy} = R_s\mu_0M) \qquad (3)$$

where R_0 is the ordinary Hall coefficient and R_s the AHE coefficient. The induction field $\mathbf{B} = \mu_0[\mathbf{H} + (1 - N)\mathbf{M}]$ is the sum of the applied field $\mathbf{H}$ and the magnetization $\mathbf{M}$ reduced by the factor $(1 - N)$, where N is the demagnetization factor ($N \sim$ 0.7-0.95 with $\mathbf{H}$ normal to the plate-like crystals).

The anomalous Hall resistivity ρ'_{xy} is the main quantity of interest in Eq. 3. As shown in Fig. 5, it is obtained by subtracting the linear background (representing R_0B) from the measured ρ_{xy} (note that the demagnetization factor N is irrelevant to ρ'_{xy}). After ρ'_{xy} is obtained, it is found to match (up to a scale factor) the profile of $M(T)$ vs. H measured at the same T. The scale factor gives the AHE coefficient $R_s(T)$ which is plotted against T in Fig. 3 (main text) for each sample.

Below T_C, the ordinary Hall coefficient R_0 is technically difficult to determine from the linear background term R_0B because it is enhanced by the term $M(1-N)$. In addition, a significant H-linear term may arise from the so-called "paraprocess" susceptibility $\partial M/\partial H$ (which is amplified if $R_s \gg R_0$). These contributions are hard to estimate accurately (*Ref. 1, p. 158*). As in standard practice, we have measured R_0 at temperatures near T_C or above it and assumed that the hole density $n_h = (eR_0)^{-1}$ is T independent. We note that the hole density determined is in nominal agreement with the chemical argument that each Br removes one hole per formula unit.

AHE conductivity
The total Hall conductivity σ_{xy}^{tot} is the sum of the ordinary Hall conductivity (σ_{xy}^0) and the AHE conductivity (σ'_{xy}). By matrix inversion, we then have

$$\sigma_{xy}^{tot} = \sigma_{xy}^0 + \sigma'_{xy} = \frac{\rho_{xy}}{[\rho^2 + \rho_{xy}^2]} \simeq \frac{\rho_{xy}}{\rho^2}. \qquad (4)$$

In our samples, the Hall angle ratio $\tan\theta_H = \rho_{xy}/\rho$ varies (at 5 K) from 5×10^{-3} at $x = 0.1$ to 2×10^{-2} at $x = 1.0$. Hence at any x, the correction $(\rho_{xy}/\rho)^2$ is negligibly small. This justifies its neglection in the second step (this seems the case for all published Hall results on ferromagnets). Identifying σ_{xy}^0 with R_0B/ρ^2, and comparing Eqs. 3 with 4, we obtain for the AHE conductivity

$$\sigma'_{xy} = \rho'_{xy}/\rho^2. \qquad (5)$$

By Eq. 5, if $|\rho'_{xy}|/n_h$ is proportional to ρ^2, the magnitude of the normalized AHE conductivity $|\sigma'_{xy}|/n_h$ is independent of τ.

Magnetoresistance
At the saturation field when domains become aligned, the elimination of domain walls leads to a slight reduction in carrier scattering which is observed as a negative

magnetoresistance (MR). This MR does not affect the extraction of ρ'_{xy} (since it is symmetric in H), but it comes in when we calculate σ'_{xy} from Eq. 5. However, in all our samples, the negative MR is a 1-2 % effect (Fig. 5B). Inclusion of this small MR correction to ρ leads to a change that is unresolvable in Fig. 4.

Resolution

For samples with $x \geq 0.5$, the relatively large AHE resistivity ρ'_{xy} at 5 K may be measured with reasonably high accuracy. In the low-x limit, however, the steep decrease of ρ (at 5 K) causes $|\rho_{xy}|$ to fall very rapidly towards zero. We discuss our resolution in this limit. Figure 6
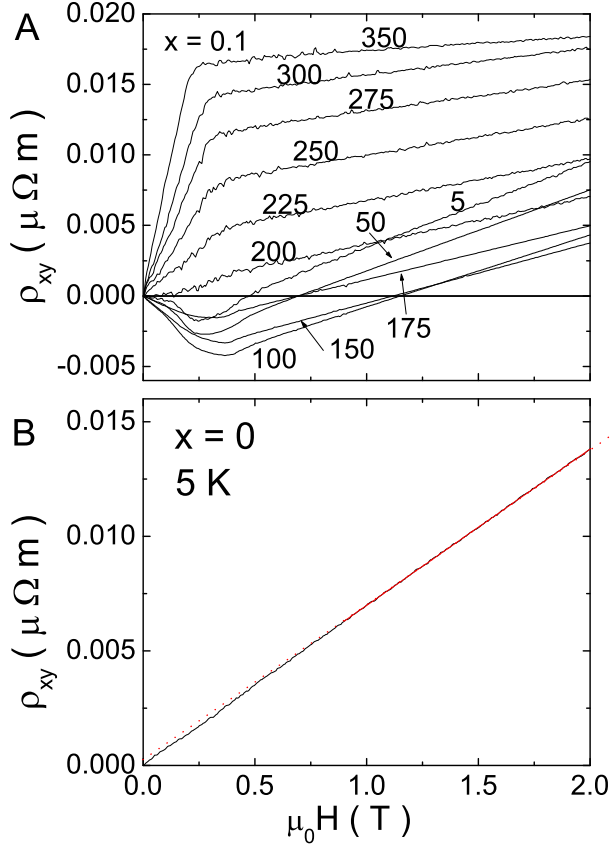

FIG. 6: (Panel A) Curves of the observed Hall resistivity $\rho_{xy} = R_0 B + R_s \mu_0 M$ vs. H in $CuCr_2Se_{4-x}Br_x$ with $x = 0.10$. R_s changes from positive to negative as T falls below 180 K, and rapidly decreases in magnitude. However, it remains clearly resolvable at 5 K. Panel B shows the curve of ρ_{xy} vs. H in the sample with $x = 0$ at 5 K. The close fit to a straight line (red dashed line) implies that ρ'_{xy} is below our resolution in this sample.

compares the curves of ρ_{xy} measured in a sample with $x = 0.10$ (Panel A) with one at $x = 0$ (B). In Panel A, the AHE component ρ'_{xy}, with its characteristic 'knee' profile is readily distinguished at high T. As T decreases below 175 K, R_s becomes negative. Further, as T decreases, the slope of the background term $R_0 B$ increases noticeably,

an effect commonly observed in ferromagnets. Despite the large $R_0 B$ term at low T, the knee profile of ρ'_{xy} remains clearly resolved down to 5 K. This is the lowest data point displayed in Fig. 4

The undoped sample ($x = 0$) provides a quantitative test of our resolution. Panel B shows the raw trace of its ρ_{xy} vs. H at 5 K, in which the AHE signall is not resolved. The data above 0.7 T fit very closely to a straight line (dashed red line). From the small intercept of the fit at $H = 0$, we estimate an upper bound ($|\rho'_{xy}| < 2 \times 10^{-10}$ Ωm) for the AHE signal. Because the AHE signal at 5 K is unresolved, the $x = 0$ sample is not displayed in Fig. 4. Significantly, however, the upper bound (which implies that $|\rho'_{xy}|/n_h < 2.8 \times 10^{-38}$ Ωm^4) is consistent with the best linear fit in Fig. 4. The value of $|\rho'_{xy}|/n_h$ predicted by extrapolating the straight-line fit to the value of ρ ($= 24$ $\mu\Omega$cm at 5 K) in this sample would fall slightly below our resolution. This illustrates the problem of measuring $\rho'_{xy} = \sigma'_{xy}\rho^2$ in high-purity ferromagnets at low T. Even if σ'_{xy} is sizeable, ρ may be too small to render ρ'_{xy} observable.

References and Notes

1. *The Hall Effect in Metals and Alloys*, ed. Colin Hurd (Plenum, New York 1972) p. 153.
2. L. Berger, G. Bergmann, *The Hall Effect and Its Applications*, ed. C. L. Chien, C. R. Westgate (Plenum, New York 1980), p. 55.
3. R. Karplus, J. M. Luttinger, *Phys. Rev.* **95**, 1154 (1954).
4. J. M. Luttinger, *Phys. Rev.* **112**, 739 (1958).
5. E. N. Adams, E. I. Blount, *J. Phys. Chem. Solids* **10**, 286 (1959).
6. J. Smit, *Physica (Amsterdam)* 21, 877 (1955).
7. L. Berger, *Phys. Rev. B* **2**, 4559 (1970).
8. S. K. Lyo, T. Holstein, *Phys. Rev. B* **9**, 2412 (1974).
9. P. Nozières, C. Lewiner, *J. Phys. (France)* **34**, 901 (1973).
10. M. Onoda, N. Nagaosa, *J. Phys. Soc. Jpn.* **71**, 19 (2002).
11. T. Jungwirth, Qian Niu, A. H. MacDonald, *Phys. Rev. Lett.* **88**, 207208 (2002).
12. H. Ohno, *Science* **281**, 1660 (1998).
13. P. Matl *et al.*, *Phys. Rev. B* **57**, 10248 (1998).
14. J. Ye *et al.*, *Phys. Rev. Lett.* **83**, 3737 (1999).
15. Y. Taguchi *et al.*, *Science* **291**, 2573 (2001).
16. J. E. Hirsch, *Phys. Rev. Lett.* **83**, 1834 (1999).
17. S. Murakami, N. Nagaosa, S. C. Zhang, *Science* **301**, 1348 (2003).
18. C. Kooi, *Phys. Rev.* **95**, 843 (1954).
19. W. Jellinghaus, M. P. DeAndres, *Ann. Physik* **7**, 189 (1961).
20. J. Smit, *Phys. Rev. B* **8**, 2349 (1973).
21. S. K. Lyo, *Phys. Rev. B* **8**, 1185 (1973).
22. K. Miyatani *et al.*, *J. Phys. Chem. Solids* **32**, 1429 (1971).
23. J. B. Goodenough, *J. Phys. Chem. Solids* **30**, 261 (1969).
24. See Supporting Online Material.
25. F. Ogata, T. Hamajima, T. Kambara, K. I. Goondaira, *J. Phys. C.* **15**, 3483 (1982).
26. R. J. Soulen Jr. *et al.*, *Science* **282**, 85 (1998).
27. G. Schmidt, D. Ferrand, L. W. Molenkamp, A. T. Fiolip, B. J. van Wees, *Phys. Rev. B* **62**, R4790 (2000).
28. We acknowledge support from a MRSEC grant (DMR 0213706) from the U. S. National Science Foundation.

Supporting Online Material
www.sciencemag.org
Materials and Methods